Research Article

Received: 29 September 2009 Revised: 8 January 2010 Accepted: 19 January 2010 Published online in Wiley Interscience: 29 March 2010

(www.interscience.wiley.com) DOI 10.1002/jctb.2370

Photovoltaic solar electrochemical oxidation (PSEO) for treatment of lignosulfonate wastewater

Antonio Dominguez-Ramos,* Ruben Aldaco and Angel Irabien

Abstract

BACKGROUND: Under the current global energy scenario, the need for self-sustainable processes is encouraged. The photovoltaic solar powered electrochemical oxidation (PSEO) process has been developed to remove the organic matter from a lignosulfonate wastewater.

RESULTS: An electrochemical reactor using boron-doped diamond electrodes, in a batch configuration, is directly supplied with current from a set of photovoltaic solar modules. Experimental results show that the process can oxidize about 90% of the total organic carbon (TOC) of the organic matter in the wastewater under the described operating conditions.

CONCLUSION: The technical suitability of the PSEO process has been demonstrated. A model to relate solar irradiance and electrical current was applied and used in a kinetic expression which depends on solar irradiance to describe the removal of TOC.

Keywords: electrochemical oxidation; kinetics; mathematical modelling; photovoltaic solar energy; diamond boron-doped electrodes; lignosulfonate

NOTATION

- A_E = Total electrode area (cm^2)
- A_M = Total area of photovoltaic modules (m^2)
- C = Concentration of organic matter expressed as total organic carbon ($mgC\ L^{-1}$)
- C_0 = Initial concentration of organic matter expressed as chemical oxygen demand ($mgO_2\ L^{-1}$)
- E_C = Energy collected by the set of solar modules (kW h)
- E_U = Energy used in the electrochemical reactor for the oxidation of organic matter (kW h)
- $E_{SC,m}$ = Specific energy consumption used in the electrochemical reactor per unit of mass (kW h mgC)
- $E_{SC,v}$ = Specific energy consumption used in the electrochemical reactor per unit of volume ($kW\ h\ m^{-3}$)
- G = Global irradiance on the plane of the photovoltaic modules ($W\ m^{-2}$)
- g = Incident solar power on the plane of the photovoltaic modules (W)
- g_{AV} = Average incident solar power on the plane of the photovoltaic modules (W)
- I = Total current generated by the set of photovoltaic modules per total module area ($A\ m^{-2}$)
- i = Total current generated by the set of photovoltaic modules (A)
- i_{AV} = Average total current generated by the set of photovoltaic modules (A)
- i_C = Total applied current under controlled conditions (mA)
- $i_{MP,ref}$ = Current provided by the photovoltaic module at the maximum power point and standard conditions of irradiance ($1000\ W\ m^{-2}$) and module temperature (25 °C) at AM1.5 (A)
- $i_{SC,ref}$ = Current provided by the photovoltaic module under short-current and standard conditions of irradiance ($1000\ W\ m^{-2}$) and module temperature (25 °C) at AM1.5 (A)
- J = Current density ($mA\ cm^{-2}$)
- K = Instantaneous kinetic constant as a function of g ($m\ min^{-1}$)
- K_1 = Parameter for the assessment of the reaction rate as a function of g ($m\ min^{-1}\ A^{-1}$)
- K_2 = Parameter for the assessment of the reaction rate as a function of g (A^{-1})
- K_{exp} = Apparent kinetic constant obtained by linear fitting of TOC removal values ($m\ min^{-1}$)
- K_m = Mass transfer coefficient in the electrochemical reactor ($m\ min^{-1}$)
- K_{max} = Maximum observed kinetic constant for TOC removal (min^{-1})

* *Correspondence to: Antonio Dominguez-Ramos, Departamento de Ingeniería Química y Química Inorgánica, Universidad de Cantabria, Avda. de Los Castros, s/n, 39005, Santander, Spain. E-mail: domingueza@unican.es*

Departamento de Ingeniería Química y Química Inorgánica, Universidad de Cantabria, Avda. de Los Castros, s/n, 39005, Santander, Spain

K_ϑ = Kinetic constant expressed as a function of ϑ (m min^{-1})
N_{PV} = Number of connected photovoltaic modules (–)
$-r_A$ = Reaction rate referred to the electrode area (mgC m min^{-1} L^{-1})
t_{OP} = Number of minutes of operation to achieve a 90% removal expressed as TOC (min)
v_E = Electrochemical reactor volume (L)
$v_{OC,ref}$ = Voltage provided by the photovoltaic module in open circuit and standard conditions of irradiance (1000 W m^{-2}) and module temperature (25 °C) at AM1.5 (V)
$v_{MP,ref}$ = Voltage provided by the photovoltaic module at the maximum power point and standard conditions of irradiance (1000 W·m^{-2}) and module temperature (25 °C) at AM1.5 (V)
v_S = Solution volume (L)
α^* = Fitting parameter for batch data under controlled current condition (mgO_2 m mA^{-1} min^{-1})
β^* = Fitting parameter for batch data under controlled current condition (mgO_2 mA^{-1})
λ = Conductivity of the effluent (mS cm^{-1})
ϑ = Applied current per mass of O_2 (mA mgO_2^{-1})
η = Power conversion efficiency by the set of photovoltaic modules (%)

INTRODUCTION

Now that mankind is facing great challenges with the supply of energy, water and food one of the most important for societies all over the world more especially if we still continue to live with energy generation based on fossil fuels, which is a main element in climate change.[1] The integration of renewable energy sources not only in power generation but in other production systems is a key challenge, as noted in *A Roadmap for the 21th Century Chemical Engineering* by the Institution of Chemical Engineers.[2]

Photovoltaic solar conversion energy is based on the separation of charges at the interface of two materials with different conduction mechanisms.[3] Solid-state devices such as those based on monocrystalline silicon materials, under light irradiation have the capacity to absorb a fraction of the energy carried by the device surface, displacing photons into electrical current carriers, i.e. electrons and holes.[4] Monocrystalline silicon materials can be obtained by the energy-intensive Czochralski process. This crystallographic structure is desirable due to the reduction in the number of grains in the material, the borders of which act as defects and therefore reduce the efficiency of the material.[5] As photovoltaic technology matures there is the prospect of low-cost production processes and almost zero nett CO_2-eq emissions throughout the life cycle;[8,9] thus, the integration of these energy devices into processes and applications related to chemical technology and water treatment should be considered in the mid-term range.

Different research studies using solar energy devices for water treatment have been undertaken, as summarized in Table 1. Electrocoagulation with Fe^{3+} powered by photovoltaic solar energy was studied,[10] with the flow rate treated as a function of the instantaneous solar irradiance; photovoltaic solar energy was also used to supply the current required to produce Fenton's reagent in a divided cell with reticulated vitreous carbon anodes, and used to oxidize different dyes and real effluents.[11] Electrochemical combustion of organics using BiO_X–TiO_2 anodes can improve hydrogen production in stainless steel cathodes.[12] It is worth mentioning that the references in Table 1 indicate that different processes using electricity can use photovoltaic technology in an autonomous way. Direct supply from photovoltaic modules is well established and electrochemical oxidation processes can gain advantages from being supplied by photovoltaic energy. The key issues that encourage proper use of water treatment processes powered by photovoltaic energy can be summarized as follows:

- No need for energy storage systems. The processes can be designed in such a way that solar irradiation is transformed into electricity and used as input for electrochemical oxidation: it is simpler and provides cheaper clean water than other equivalent energy systems (e.g. lead acid batteries).[13]
- Direct supply to the treatment process, which implies that the flow can be treated in a continuous system as a function of solar irradiance

Wastewater treatment leading to the removal of organic matter, such as electrochemical oxidation (EO) based on boron-doped diamond electrodes has been claimed as an advanced technology in purification and disinfection applications, promoting water reclamation and close-to-zero nett use of water from natural resources. The reduction of sludge and consumption of chemicals are very attractive features of EO when compared with biological processes. When an electrical current is applied to the electrodes, powerful oxidants are created in the surface or the bulk liquid phase, depending on the operating conditions, promoting oxidation of the organic matter to CO_2 and H_2O. Nevertheless,

Table 1. Photovoltaic powered processes for wastewater treatment

Coupled process	Direct connection to PV supply	PV installation characteristics	Water treatment unit characteristics	Reference
Electrocoagulation	Yes	1 × PQ10/40/01-02 AEG of 38.48 W_P (poly-crystalline silicon)	Total anodic area: 235 cm^2 (central aluminium anode between two stainless steel cathodes)	10
Oxidation with Fenton's reagent	Yes (voltage regulator)	1 × solar panel (50 W; 17 V; 2.9 A; Syscom Inc. Model BP 350U)	3D-RVC electrode (5 cm × 5 cm × 1 cm); 60 pores per inch; fitted into centre of catholyte channel; Nafion® 117 cation permeable membrane separator; stainless steel gauze anode (5 cm × 5 cm) and silicon rubber gaskets	11
Electrochemical Oxidation	Yes	4 × 160 W_P SunTech (monocrystalline; total rating 640 W_P)	70 cm^2 BDD electrodes single-compartment flow cell	This work

this technology has the major drawback of high electrical energy demand per unit of treated volume,[14] which can be avoided by using renewable energy sources.

The aim of this work is to show the technical feasibility of a photovoltaic solar powered electrochemical oxidation process (PSEO) to remove organic matter from a lignosulfonate solution by performing an energy and mass balance to the coupled process, in order to describe the experimental results.

MATERIALS AND METHODS

A synthetic solution of calcium and magnesium lignosulfonate was prepared as typical biorefractory organic matter to test the reliability of the PSEO process. To prepare the lignosulfonate solutions a commercial Borrebond 55S calcium-magnesium lignosulfonate (molecular weight about 3000 daltons) from *Eucalyptus globulus* (sulfite process) was obtained from Lignotech Iberica S.A. (Torrelavega, Spain). This product is water soluble and has a residual concentration of reduced sugars. It was used as received without additional purification. Sodium sulfate from Panreac Quimica SA was added as a supporting electrolyte to maintain conductivity between the electrodes. A total solution volume (v_S) of 2 L with the required quantity of lignosulfonate and sodium sulfate in ultrapure water (Milli-Q) was used in each experiment.

Lignosulfonate solutions were introduced in a single compartment flow electrochemical reactor (Adamant Technologies SA) operating in a semi-batch mode. The experimental setup is shown in Fig. 1. The external parts of the reactor are made of polypropylene and tightened to prevent leakages. The electrochemical reaction takes place in the cell: the anode and cathode are based on conductive thin-films of boron-doped diamond (active layer with a thickness in the range 1–3 µm and a total resistivity of 100–150 mΩ cm) supported on a silicon substrate (p-silicon with a thickness of 2 mm and a total resistivity of 100 mΩ cm). The electrodes have a parallel configuration characterized by an inter-electrode gap of 1 mm. Anode and cathode are both circular with a total wet area (A_E) of 70 cm^2 per electrode (during the different experiments no alteration of the active surface was noticed). A centrifugal pump was used to circulate the solution through the electrochemical cell, with flow-rate measured by rotameter. Up to four monocrystalline photovoltaic modules (SunTech Co. Ltd. STP160) were connected giving a total peak power of 640 W_P from an effective area of 1.125 m^2 per module (see Table 2 for details). Photovoltaic modules were placed on the roof of ETSIIyT, University of Cantabria, Santander, Spain (W3°47′52.17″, N43°28′22.33″) tilted at 38° and south orientation (20° West). The set of modules were directly connected to the electrochemical reactor through a fuse box. No shadowing effect was noted during the experiments.

Table 3 summarizes relevant operating conditions in the experiments. All experiments began at 10:30 PM (local time) enabling the connection of the photovoltaic modules to the electrochemical reactor: the operating time t_{OP} was extended to guarantee that TOC removal around 90% was obtained. Flow-rate through the electrochemical cell was kept constant at 300 L h^{-1}. The temperature of the solution was maintained constant between 22 and 24 °C for the selected experiments (except for E2 at 32 °C). Samples were withdrawn from the solution tank at regular times. The objective of the set of experiments shown in Table 3 was to demonstrate the technical viability of a PSEO process to remove TOC from a lignosulfonate solution under different solar irradiance conditions and initial concentrations, and to obtain experimental

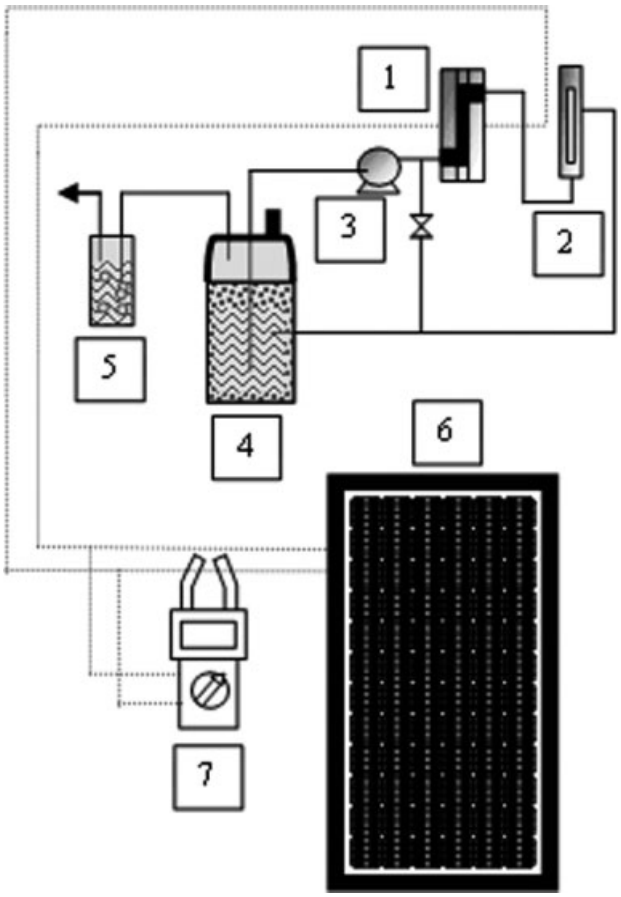

Figure 1. Experimental set-up. 1. Single compartment flow electrochemical reactor Power supply, 2. Flowmeter, 3. Centrifugal pump, 4. Refrigerated glass tank, 5. Absorber, 6. Photovoltaic modules 7. Unit for measurement of current and voltage.

Table 2. Characteristics of the SunTech photovoltaic module STP160

Parameter	Value	Units
$i_{SC,ref}$	5	A
$v_{OC,ref}$	43.2	V
$i_{MP,ref}$	4.65	A
$v_{MP,ref}$	34.4	V

data to perform the energy and mass balances in the system and to scale up the water treatment.

Total organic carbon (TOC) of each sample was analysed using a Shimadzu TOC-V CPH with ASI-V, operating with synthetic air from Air Liquide S.A., Spain (pressure 200 kPa; flowrate: 150 mL min^{-1}). Both pH and conductivity were measured (values corrected to 25 °C) using a Hach HQ40d unit (Hach Lange). Solar irradiance time profiles were measured at intervals of 15 min using a SunReader unit (SunTechnics Conergy Group). To obtain current, voltage and power time profiles a Fluke 345 unit was used for measurements and recording (logged at intervals of 10 s and displayed at intervals of 15 min after resampling). This unit is able to measure the input current in the electrochemical cell generated by the set of photovoltaic modules in each experiment and the applied voltage between electrodes, i.e. the output voltage of the photovoltaic

Table 3. Experimental conditions

Exp	Date	N_{PV} –	t_{OP} min	C_0 mgC L^{-1}	Supporting electrolyte $[Na_2SO_4]$ g L^{-1}
E1	29-04-2008	2	300	624	2.5
E2	05-05-2008	4	240	700	2.5
E3	07-05-2008	2	300	200	2.5
E4	15-05-2008	1	480	656	0.3

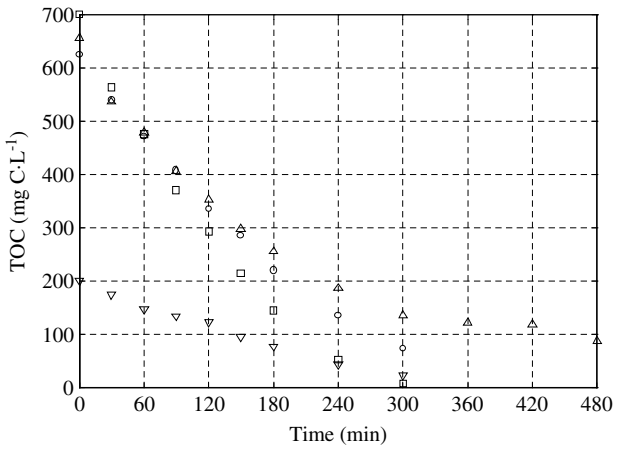

Figure 2. Evolution of total organic carbon versus time. (○) E1; (□) E2; (▽) E3; (△) E4.

modules. Once the power profile is available, it is possible to evaluate the energy applied to the electrochemical system. All analytical and electrical measurements were in good agreement with expected relative errors from the specified values.

RESULTS AND DISCUSSION

Evolution of total organic carbon

Figure 2 shows the time profile of TOC for the set of experiments, from which it is clear that the PSEO process is able to remove the organic matter from a lignosulfonate solution. As previously stated, the experiments were extended until relevant data for the kinetic analysis were available. Consequently, higher yields than those presented here could be obtained simply by extending the operation time. Details of the mass balance and the kinetics of the process are discussed later.

Energy analysis

It is important to complete analysis of the energy input to the electrochemical system. Figure 3 shows the time profiles for incident solar power (g) (solar irradiance on the plane defined by the position of the photovoltaic modules G multiplied by the corresponding effective module area A_M) and the total output current (i) (inset of Fig. 3). The maximum experimental value of incident solar power (g) was 4.53 kW and total output current (i) 19.8 A. It can be seen that the higher values of g were obtained for E2, which was operating under clear sky conditions with the maximum number of photovoltaic modules (4) connected in parallel, (Table 3). In contrast, lower values of g were obtained for E4, when only one photovoltaic module was connected and clouds appeared during the experiment. To check the experimental

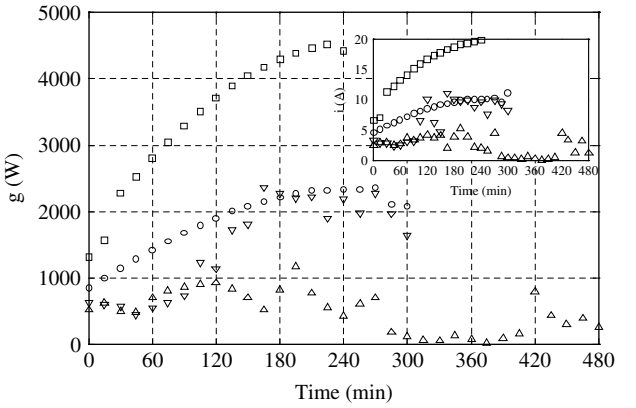

Figure 3. Incident solar power $g = GA_M$ versus time. (○) E1; (□) E2; (▽) E3; (△) E4. Inset: evolution of total applied current i versus time. (○) E1; (□) E2; (▽) E3; (△) E4.

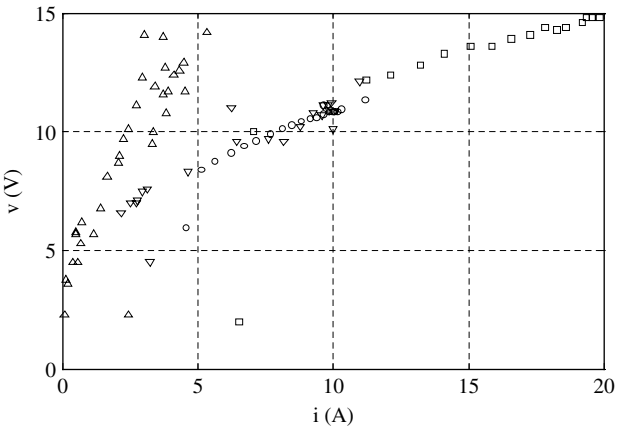

Figure 4. Voltage between electrodes v versus input current i: (○) E1; (□) E2; (▽) E3; (△) E4.

results, the maximum irradiance under clear sky conditions was used as reference. From the photovoltaic geographical information system (PVGIS) of the Joint Research Centre of the European Commission (http://re.jrc.ec.europa.eu/pvgis), accessed in 2009, a maximum daily value of global clear sky solar irradiance of 981 W m^{-2} was obtained for May (tilt of 38° and south orientation (20 °W)) in Santander, so the theoretical maximum value of g was 4.42 kW. Consequently, differences from the maximum values from PVGIS were below 3%, which agrees well with the experimental results.

Once consistent energy input is confirmed, it is of interest to relate the generated current directly applied to the electrochemical reactor to the corresponding voltage. In Fig. 4, the relationship between the voltage between electrodes (v), which is equal to the photovoltaic modules voltage, and the applied current (i) is shown. As can be seen in Fig. 4, there is no nett current through the system until a value around 5 V is reached, and then a linear relationship between v and i is observed. The slope is the ohmic resistance of the electrochemical reactor, which is mainly due to the conductivity of the solution pumped between the electrodes. Therefore, two different curves can be distinguished in Fig. 4: the curve for E4, which has the higher ohmic resistance due to the lower concentration of supporting electrolyte and therefore the lower conductivity, and the curves for E1–3, which have the

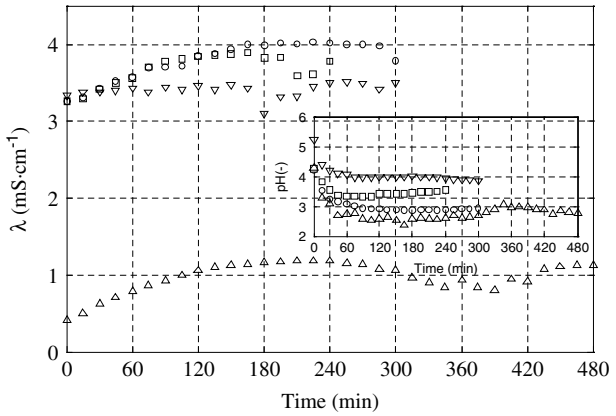

Figure 5. Conductivity of the solution for experiment: (○) E1; (□) E2; (▽) E3; (△) E4. Inset: pH of the solution for experiment (○) E1; (□) E2; (▽) E3; (△) E4.

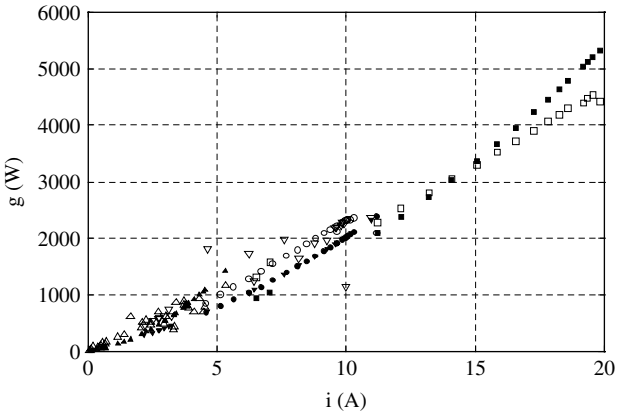

Figure 6. Incident solar power *g* versus total applied current *i* for experiments: (○) E1; (□) E2; (▽) E3; (△) E4 and calculated values (●) E1; (■) E2; (▼) E3; (▲) E4.

same supporting electrolyte concentration and therefore similar ohmic resistances. Values of *v* as a function of *i* were fitted to the relationship shown in the equation:

$$v = v_0 + iR \tag{1}$$

This expression is frequently used for electrochemical purposes with v_0 the minimum required voltage to generate a nett current in the system.[15,16] The v_0 value was 3.89 ± 1.15 V for E4 and 5.70 ± 0.69 V for the set of curves E1–3. The slope was $R = 2.10 \pm 0.40\ \Omega$ for E4 and $R = 0.50 \pm 0.06\ \Omega$ for the set of curves E1–3. Corresponding values of R^2 for E4 and the set for E1–3 were $R^2 = 0.79$ and 0.81, respectively. Consequently, the relation between *v* and *i* is influenced by the ohmic resistance due to the solution conductivity. Figure 5 shows the conductivity profile in the experiments. Conductivity shows an asymptotic behaviour, starting from $\lambda = 3.3\ \text{mS cm}^{-1}$ up to a stationary value around $\lambda = 3.5\text{–}4\ \text{mS cm}^{-1}$ for E1–3. On the other hand, for E4, at the beginning of the experiment the conductivity was only $\lambda = 0.4\ \text{mS cm}^{-1}$ (as the minimum quantity of sodium sulfate was added to the solution) and an increase was observed up to values $\lambda = 1.0\ \text{mS cm}^{-1}$. Therefore, stationary conductivity values are obtained after the first hour of operation. A relationship between solution conductivity and ohmic resistance is also observed due to the fact that increasing the conductivity four-fold (from $\lambda = 1.0\ \text{mS cm}^{-1}$ to $\lambda = 3.5\text{–}4\ \text{mS cm}^{-1}$) approximately decreases the ohmic resistance four times (from $R = 2.1\ \Omega$ to $R = 0.5\ \Omega$). Figure 5 shows the pH time profile: initial values of pH were around pH = 4.25 for E1-2-4 due to the same initial concentration of lignosulfonate and pH = 5.22 for E3; in this experiment the higher initial value was obtained due to the lower concentration of lignosulfonate, which has an acidic behaviour. A sharp decrease up to stationary values around pH = 3, 3.5, 2.75 was observed, respectively, for E1, 2, 4. For E3, a sharp decrease is also observed up to stationary values of pH = 4. Therefore, it is observed that the pH values tend to reach a stationary value. Therefore, it could be stated that pH and conductivity should present stationary behaviour under operation with stochastic input current. Additionally, a correlation between pH and conductivity is observed: the increase in the concentration of protons (H^+) increases the conductivity due to the high proton molar conductivity compared with other dissolved species[17] such as carbonic acid.

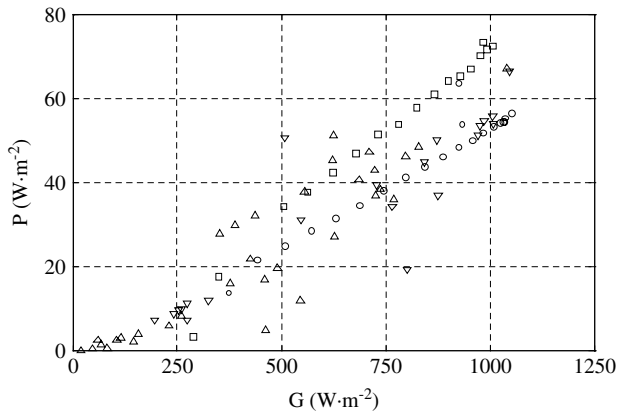

Figure 7. Electrical power per unit of module area *P* versus solar irradiance *G* for experiments: (○) E1; (□) E2; (▽) E3; (△) E4.

Equation (1) makes it possible to relate the voltage between electrodes and the applied current, but of interest is the relationship with the incident solar power (*g*). It can be observed from Fig. 4 that *i* follows the same trend as *g*, so the incident solar power (*g*) is plotted versus generated current (*i*) (Fig. 6), from which a linear relationship for low values of *g* and a positive deviation as *g* increases can be seen. Consequently, there is a relationship between these variables that should consider the fact that at high *g* values the relationship is no longer linear. Figure 7 shows the evolution of electrical generated power per module area unit (*P*) versus the incident solar power per module area unit or solar irradiance (*G*), and as can be seen from this figure, a linear relationship is observed between *P* and *G*. This relationship should be related to the conversion efficiency of the modules. The power conversion efficiency (η) is defined at the maximum power point.[4] For a point different from the maximum power point, the corresponding slope in the linear relationship between *P* and *G*, as shown in Equation (2) gives the power conversion efficiency:

$$\eta = \frac{P}{G} = \frac{pA_M^{-1}}{gA_M^{-1}} = \frac{p}{g} = \frac{Iv}{G} \tag{2}$$

The module efficiency is presented in Table 4, showing that a higher value of η is obtained for E2, which is the experiment in which the higher number of modules was connected and the

Table 4. Energy variables and efficiency in the experiments

Exp	E_C kW h	E_U kW h	η %
E1	9.42	0.59	5.3
E2	13.85	1.14	7.0
E3	7.46	0.37	5.3
E4	4.03	0.20	5.6

Table 5. Specific energy consumption in the experiments

Exp	$E_{SC,m}$ kW h kgC^{-1}	$E_{SC,v}$ kW h m^{-3}
E1	534	294
E2	882	571
E3	1035	184
E4	176	100

minimum ohmic resistance was observed. However, no influence of the number of modules or ohmic resistance was observed for the whole set of experiments. As shown in Table 4, the efficiency of the set of modules η is around 5–7% for the experiments, which is still far from the values for modules efficiency ($\eta = 14.2\%$) and the typical 15% of current monocrystalline silicon photovoltaic modules.[7] Therefore, it is possible to make a better use of the energy collected, which should be based on adjusting the load of the electrochemical reactor to the corresponding maximum power point of the module.[5] The combination of Equations (1) and (2) provides the following relationship between g and i:

$$g = \frac{p}{\eta} = \frac{iv}{\eta} = \frac{i(v_0 + iR)}{\eta} = \frac{iv_0 + i^2R}{\eta} \tag{3}$$

where for low values of i

$$g \approx \frac{v_0}{\eta} i$$

and for high values of i

$$g \approx \frac{R}{\eta} i^2$$

So if v_0, R and η are known for the system, the solar irradiance (G) gives the input current (i) to the system and using Equation (1) the voltage can easily be obtained. The electrical power (p) considers two terms: the electrical use for electrochemical purposes and thermal losses due to the Joule effect. From Equation (3) it can be seen clearly that if R is increased due to a lower effluent conductivity, a higher solar power g is then required to obtain similar input current (i) values. Full dots in Fig. 6 show the values obtained for g when calculated using Equation (3) with the previous experimental values for v_0, R and η; although some deviations are presented they are consistent with the implicit error when the values of the parameters v_0, R and η are used, so an acceptable agreement between calculated and experimental values is observed.

An energy analysis based on the i–v relationship has been performed and with the corresponding values of v_0, R and η, the variation of the electrical variables of the electrochemical system can be obtained as a function of the irradiance (G). The basis of modelling the output current (i) and voltage (v) from photovoltaic modules as a function of the solar irradiance (G) is available in several references[18–20] and specific references applied in the area of wastewater treatment processes are also available.[21,22] The complexity of the relationship between current and voltage for the solar module depends on the selected model. A well-known model is the five parameters model, details of which can be found elsewhere.[18,19] In this work the energy analysis relating the input current (i) and the solar power (g) as shown in Equation (3) agrees well with experimental data and it will be applied for the process modelling.

Finally, it is important to complete the energy analysis by checking how efficiently the available energy is used for the electrochemical oxidation of the organic matter. To improve cross-checking between references, the concept of energy per order[23] was avoided as it is difficult to make explicit the order of the individual kinetics, i.e zero or first order, in each reference and especially for the experiments, where the random nature of the solar irradiation could make the process move from one order to another. Table 4 shows the energy data related to the experiments. The expression to calculate the total collected energy E_C in each experiment is

$$E_c = \int_0^t g dt \tag{4}$$

Therefore E_C is calculated from integration of the incident solar power over the period corresponding to the total duration of the experiment. As deduced from Table 4, the maximum energy collected $E_C = 13.85$ kWh was for E2, as the number of modules connected was the maximum available under clear sky conditions. On the other hand, the total electrical energy E_U in each experiment is calculated from

$$E_U = \int_0^t ivdt \tag{5}$$

The values of E_U account for the energy applied to the electrochemical reactor oxidize the organic matter and the thermal losses due to the Joule effect. In a parallel way to Equation (4), E_U is calculated by integration of the energy used over the total duration of the experiment. The maximum utilization of energy also took place in E2.

Once the energy E_U is available, it is of interest to calculate two ratios to assess how efficiently the energy is used for organic matter removal. In Table 5 the specific energy consumption in each experiment is summarized, expressed as the energy required to remove a unit of mass $E_{SC,m}$:

$$E_{SC,m} = \frac{\int_0^t ivdt}{v_s \Delta [TOC]_0^t} \tag{6}$$

or the energy to remove the organic matter per volume unit $E_{SC,v}$:

$$E_{SC,v} = \frac{\int_0^t ivdt}{v_s} \tag{7}$$

From Table 5, despite having the lower concentration of supporting electrolyte, it is clear that the experiment E4 required a lower specific energy consumption ($E_{SC,m}$) of 176 kW h kgC^{-1}. For the other experiments, $E_{SC,m}$ ranges from 534–1035 kW h kgC^{-1}. In order to compare the estimated values of energy consumption, several references are provided in Table 6 for synthetic and real effluents. For phenol removal with BDD electrodes, values

Table 6. Specific energy consumption in electrochemical oxidation from the literature

Type of origin	Effluent	$E_{SC,m}$ kW h kgC^{-1}	$E_{SC,v}$ kW h m^{-3}	Comments	Ref.
Synthetic	Phenol	26-91		BDD electrodes (initial TOC: 400–1000 mgC L^{-1}; 5000 mg Na_2SO_4; current densities: 15–60 mA cm^{-2})	14
Real	Urban wastewater		0.7	Conventional treatment	24–26
Real	Fenton - refractory	94	150	BDD electrodes (initial COD: 700 mgO_2 L^{-1}; removal of 100% of COD; 3000 mgNa_2SO_4; without additional electrolyte, the energy required is twice-fold)	27
Real	Fine chemical wastewater		200	BDD electrodes (25 mS cm^{-1}; initial COD: 6000 mgO_2 L^{-1}; removal of 90%; current densities: 15 60 mA cm^{-2})	28
Real	Textile wastewater	154-822		DSA electrodes (addition of 5.85 g L^{-1} NaCl; current densities: 20–160 mA cm^{-2})	29
Synthetic	Lignosulfonate	176	100	BDD electrodes	This work

between 26 and 91 kW h kgC^{-1} have been reported.[14] When the specific energy consumption is compared with that required to treat urban wastewaters, values around 0.7 kW h m^{-3} are well established.[24–26] On the other hand, for industrial wastewaters, values tend to be higher. For example, for a Fenton-refractory olive oil mill wastewater, values of 150 kW h m^{-3} were reported[27] and for fine chemical plant wastewaters less than 200 kW h m^{-3}.[28] The degradation of textile effluents by DSA electrodes required between 154 and 822 kW h kgC^{-1} and a high concentration of sodium chloride as supporting electrolyte.[29] It can be concluded that the energy consumption for this process is of the order of magnitude of electrochemical oxidation and energy consumption depending on the removal, which is a function of applied current and effluent conductivity.

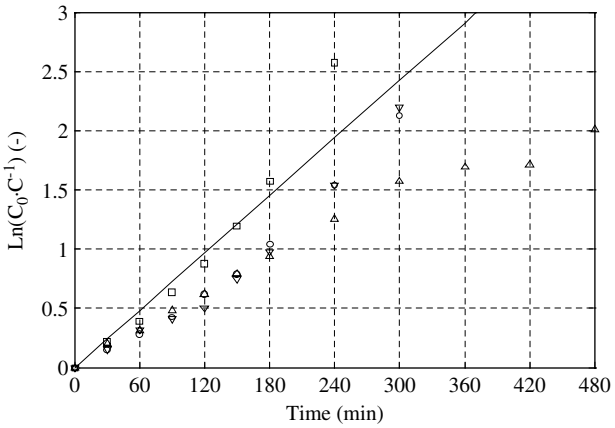

Figure 8. Organic matter removal versus time for experiments: (○) E1; (□) E2; (▽) E3; (△) E4. (—) K-line. The K-line represents the theoretical maximum removal rate obtained under controlled current conditions.

Mass balance

The energy balance was completed as a prior step to the mass analysis; discussion of the experimental results for the mass balance requires a previous analysis of the use of the energy because it is assumed that the evolution of the removal of organic matter depends on the solar irradiance. For the experiments performed, TOC removal, expressed as log C_0/C versus time has been plotted in Fig. 8. For a better understanding of the results, the maximum theoretical TOC removal rate is also shown as a straight line with zero crossing (K-line), whose slope is based on the maximum observed kinetic constant $K_{max} = 8.09 \times 10^{-3}$ min^{-1} reported previously for the experimental setup under laboratory controlled current conditions.[30] It was expected that all experimental points would be below the K-line as long as no other mechanism was involved. A maximum value of $K_m = 2.31 \times 10^{-3}$ m min^{-1} from previous laboratory studies was obtained, which was used as reference. The observed kinetic constant K_{exp} and corresponding standard error (95% confidence level) for each experiment according to a first-order kinetic is reported in Table 7.

To compare experiments, an average input current (i_{AV}) and solar power (g_{AV}) were defined for each experiment. It is observed that experiments E1 and E3 show similar values of the average input current, solar power and kinetic constant (K_{exp}) (Table 7). On the other hand, E2 and E4 show positive and negative deviations from these values. From Fig. 8, removal close to 90% is obtained for both experiments E2 and E4 at different numbers of hours of operation. It is observed from Fig. 8 that experimental values

Table 7. Apparent kinetic constants (standard error at 95% confidence level). The maximum kinetic was considered to be $K_{exp} = 2.31 \times 10^{-3}$ m min^{-1}

Exp	i_{AV} A	g_{AV} kW	$K_{exp} \times 10^3$ m min^{-1}
E1	8.48	1.86	1.80 ± 0.18
E2	15.39	3.43	2.28 ± 0.20
E3	6.69	1.47	1.79 ± 0.24
E4	2.42	0.50	1.31 ± 0.09

for E2 are on the reference K-line over the first 3 h of operation. After 3 h, deviation of experimental values above the K-line is observed for the two last experimental points This deviation, only observed for E2, corresponds with the highest value of the average input current $i_{AV} = 15.39$ A and the higher value of the kinetic constant $K_{exp} = 2.28 \times 10^{-3}$ m min^{-1}. To explain this positive deviation above the K-line, it has been suggested that a mechanism in addition to the electrochemical oxidation involving hydroxyl radicals is present, which could be used to explain the behaviour for the whole set of four experiments. This mechanism assumes that two serial steps could be taking place: (i) direct oxidation by hydroxyl radicals $OH^{\cdot}$ in the layer of liquid close to the

surface of the electrode; (ii) mass transfer of organic matter from the bulk to the electrode surface. Consequently, if the reaction rate in the layer of liquid close to the electrode is fast enough, the process will be mass transfer controlled. Additionally, the indirect oxidation by electro-generated reagents (peroxodisulfates if sodium sulfate is used), whose concentration in the bulk phase depends on the applied current and for which there is no mass transfer limitations[31,32] could be contributing in a parallel way. At these values of applied current (15.39 A), the contribution of the parallel reaction by electro-generated oxidants is suggested to have a positive effect, making the reaction rate higher than those obtained for lower values, so a maximum concentration of electro-generated peroxodisulfates was expected. If this additional mechanism is considered and assuming that the higher the applied current the higher is the concentration of oxidants in the bulk phase, an increase in the applied current may lead to reaction rates over the theoretical maximum reaction rate, which only considers the two serial steps mechanism: oxidation by hydroxyl radicals at the layer close to the electrode surface and mass transfer from the bulk phase to the electrode surface. The opposite trend is observed for E4 (Fig. 8) where the experimental values are below the K-line for the whole experiment, especially after the first 5 h. In E4, lower values of input current did occur (2.42 A) and the kinetic constant $K_{exp} = 1.31 \times 10^{-3}$ m min^{-1} was also lower. Therefore, it was expected that the contribution of parallel reactions from electro-generated reagents was negligible in E4, in which the applied current had the lower values. Additionally, for the last 3 h in E4, the removal of TOC deviated from a linear behaviour suggesting the possibility of a change of the order of the kinetics from first order. As will be explained in detail later, the kinetic constant depends on the applied current; therefore, at relatively low irradiances it is expected that the process will occur under zero order kinetics.

Once the possibility of the involvement of an additional mechanism is considered for relatively high current values, it is worth checking the influence of the applied current at more moderate applied currents. Despite having different solar irradiance profiles and initial concentrations but with similar average input currents, it can be deduced from Fig. 8 that it is possible to achieve up to 90% in TOC removal in E1 and E3 as well as in E2 and E4 but for similar t_{OP}. Considering the K-line in Fig. 8, it is observed that the experimental degradation rate is below the maximum rate in both experiments ($K_{exp} = 1.80 \times 10^{-3}$ and 1.79×10^{-3} m min^{-1}, respectively, for E1 and E3) for the total experimental time. It is noticeable that despite both experiments having different solar irradiance profiles, the evolution of TOC is similar (Fig. 8). Consequently, increasing values from 6 to 9 A did not seem to show faster removal of TOC, so the contribution of parallel reactions by electro-generated reagents may have a negligible contribution as in E4 within the cited current range.

PSEO TOC removal model

In electrochemical oxidation, the key variable is the electrical current. A model of the electrochemical oxidation of lignosulfonate under laboratory controlled current conditions has been published.[30] References detailing a mechanism involving generation of hydroxyl radicals, responsible for the electro-combustion of organic matter, on the surface of boron doped diamond anodes can be found elsewhere,[33,34] and are summarized in the following equations:

$$BDD[] + H_2O \longrightarrow BDD[OH^{\bullet}] + H^+ + e^- \quad (8)$$

$$BDD[OH^{\bullet}] + R \longrightarrow BDD[] + mCO_2 + nH_2O + H^+ + e^- \quad (9)$$

In Equation (8), BDD[] represents an active site in the boron-doped diamond layer for the discharge of a water molecule and corresponding generation of a proton and an electron. On the other hand, Equation (9) shows the combustion of organic matter (R) to combustion products (CO_2 and H_2O) plus the proton and electron pair: after oxidation of R, the active site in the boron doped diamond layer is able to accept a new water molecule in the water discharge reaction. According to this reaction scheme and based on previous references for this experimental setup and lignosulfonate as organic substrate,[30] the reaction rate $-r_A$ for TOC removal is described bythe equation:

$$-r_A = K_{\vartheta} C = \frac{\alpha^* \vartheta}{1 + \beta^* \vartheta} C = \frac{\alpha^* \left(\frac{J}{C_0}\right)\left(\frac{A_E}{V_E}\right)}{1 + \beta^* \left(\frac{J}{C_0}\right)\left(\frac{A_E}{V_E}\right)}$$

$$C = \frac{\alpha^* \left(\frac{i_C}{A_E}\right)\left(\frac{C_0 v_E}{A_E}\right)^{-1}}{1 + \beta^* \left(\frac{i_C}{A_E}\right)\left(\frac{C_0 v_E}{A_E}\right)^{-1}} C \quad (10)$$

where $-r_A$ is the reaction rate referred to the electrode area; K_{ϑ} is the intensity-dependent kinetic constant; C is the concentration of the organic matter R expressed as TOC; ϑ is the applied current per mass of O_2; α^* and β^* are fitting parameters for batch data under controlled current conditions; J is the current density; C_0 is the initial concentration of the organic matter expressed as TOC in the electrochemical reactor; A_E is the electrode area; v_E is the electrochemical reactor volume; i_C is the applied current under controlled conditions. This kinetic rate in Equation (10) shows a hyperbolic influence of the applied current on the kinetic constant, thus when the applied current becomes high enough, the process becomes controlled by the mass transfer of organic matter to the electrode surface from the bulk phase. However, if the applied current is lower, the process becomes controlled by the applied current, that is, by the oxidation in the electrode surface, and the mass transfer is no longer the controlling step. Therefore, at relatively high values of i_C or ϑ, a maximum value for K_{ϑ} is obtained: the maximum observed kinetic constant K_{max}. However, in these experimental results, the stochastic nature of the solar irradiation makes the applied current changes with time. Then, as the solar irradiance is the main input variable to the process, it was suggested that an expression was needed which correlates i with g so the reaction rate could be expressed in terms of the solar irradiance (G) or solar power (g).

A relationship between g and i is shown in Equation (3) that allows the reaction rate $-r_A$ (degradation of TOC) to be expressed as a function of the solar power (g). The substitution of Equation (3) in Equation (10) leads to Equation (11), with the controlled current (i_C) substituted by the stochastic input current (i):

$$-r_A = \frac{K_1 i(g)}{1 + K_2 i(g)} c \approx KC \quad \begin{matrix} when\ K_2 i(g) >> 1 \Rightarrow K = K_1 K_2^{-1} \\ when\ K_2 i(g) << 1 \Rightarrow K = K_1 i(g) \end{matrix} \quad (11)$$

where K is the instantaneous kinetic constant as a function of g and K_1 and K_2 are parameters derived from fitting parameters for batch data under controlled current conditions α^* and β^*, initial concentration C_0 and the electrochemical cell volume v_E. For the experimental setup and initial concentration corresponded with a chemical oxygen demand (COD) around 1500 $mgO_2\ L^{-1}$ (E1-2-4) previous values are $K_1 = 6.81 \times 10^{-4}\ m\ min^{-1}\ A^{-1}$ and $K_2 = 2.95 \times 10^{-1}\ A^{-1}$ ($K_1 = 2.06 \times 10^{-3}\ m\ min^{-1}\ A^{-1}$ and $K_2 = 8.86 \times 10^{-1}\ A^{-1}$ for COD around 500 $mgO_2\ L^{-1}$ as in E3). As previously discussed, Equation (11) shows that when relatively high values of i are available, the process becomes mass transfer controlled with $K = K_1 K_2^{-1}$ and following first-order kinetics. For relatively low values of i, the process becomes controlled with current $K = K_1 \cdot i(g)$, so under this regime, the process will follow zero-order kinetics.

Advantages of PSEO process

The PSEO process is an interesting option that meets most of the requirements of self-sustainable processes for wastewater treatment. This process was justified from an economic point of view by De Lucas *et al*.[35] who stated that electrochemical oxidation could be economically competitive if flow-rates below 1 $m^3\ day^{-1}$ were treated. Indeed, electrochemical oxidation has been suggested to be even more competitive than other advanced oxidation processes.[36] The scale of solar powered systems required is of interest and tends to be low to medium size,[37] e.g. for reverse osmosis powered by solar modules of a few thousands of cubic metres per day.

The capabilities of this technology for tertiary treatment and corresponding water reuse possibilities should be mentioned even though it is outside the scope of this work. Not only is it possible to complete the disinfection of water using BDD[38,40] or metal oxide electrodes[41] up to authorized level for water reuse but to perform it with energy consumption around 2–7.8 kW h m^{-3}, depending on the microorganism and supporting electrolyte for platinum clad niobium anodes.[40] Values of 2 kW h m^{-3} have been reported for BDD electrodes in a chlorine-free phosphate medium.[39] These values are around two orders of magnitude lower than for normal wastewater treatment.

There is a lot of opportunity for improving both electrochemical and photovoltaic solar technologies. Electrochemical technologies can benefit from the combination with other technologies such as UV radiation due to synergy in the generation of hydroxyl radicals $OH^{\cdot}$.[42] On the other hand, photovoltaic modules producers are focused on reducing manufacturing costs per watt,[43] which will end on reaching parity with the grid so the economic analysis will be controlled just by the investment on the electrochemical reactor.

The specific energy consumption required by the coupled process was 100 kW h m^{-3} for E4, which is in the range of values reported previously in Table 6. To optimize the process and make better use of the collected energy, the process should adjust not only the resistance of the electrochemical reactor, assuming it remains as the controlling ohmic resistance, to the corresponding to the maximum operating point but the applied current to the stoichiometric value.[34,44] Consequently, it is possible to reduce the specific energy consumption of the coupled process in its current status for a certain effluent based on three points of interest:

- photovoltaic module configuration (number of serial and parallel modules) and total available area (total power);
- characteristics of the effluent: conductivity and load of organic matter;
- total electrode area.

Consequently, the ratio between the area of modules and the electrode area $A_M A_E^{-1}$ can be improved: the suggested trend is to decrease the module area and increase the electrode area. In this way, the degradation rate rises due to the higher availability of electrode surface to produce hydroxyl radicals $OH^{\cdot}$ and the input current to the reactor is not used in parallel mainly hydrolysis reactions.[33]

SUMMARY

The technical suitability of a photovoltaic solar electrochemical oxidation (PSEO) process to degrade organic matter from wastewater with removal yields close to 90% TOC has been demonstrated. As the PSEO process performance depends on the applied current, a model which relates the generated input current to the process as a function of incident solar power has been developed. A reaction rate model has been proposed based on the solar power, describing the process under stochastic solar irradiance and therefore, stochastic applied current. Therefore, the TOC removal depends on the electrode area (A_E) and the photovoltaic module area (A_M). Specific energy consumption was around that of cited references. Moreover, the ratio between the photovoltaic module area and electrode area $A_M A_E^{-1}$ can be largely optimized for an effluent with fixed characteristics to prevent excess applied current and therefore allow the process to perform in a sustainable way and with an appropriate investment economic cost and a friendly environmental profile.

ACKNOWLEDGEMENTS

The authors gratefully acknowledge the financial support of the Ministry of Science and Technology of Spain through the project CTM2006-00317 and the project CENIT Sostaqua.

REFERENCES

1 British Petroleum, BP statistical review of world energy June 2008 (2008). Available at http://www.bp.com (accessed in 2009).
2 IChemE, Institution of Chemical Engineers, A roadmap for the 21th century chemical engineering (2007). Available at http://www.icheme.org/roadmap2007.pdf (accessed in 2009).
3 Grätzel M, Conversion of sunlight to electric power by nanocrystalline dye-sensitized solar cells. *J Photochem Photobiol A* **164**:3–14 (2004).
4 Luque A and Hegedus S, *Handbook of Photovoltaic Science and Engineering*. John Wiley & Sons, Chichester, 1138 (2003).
5 Markvart T, *Solar Electricity, 2nd edn reproduced with corrections*. John Wiley & Sons, Chichester, 280 (2006).
6 Hoffmann W, PV solar electricity industry: market growth and perspective. *Solar Energy Mater Solar Cells* **90**:3285–2311 (2006).
7 EPIA and Greenpeace, Solar generation V-2008 solar electricity for over billion people and two million jobs by 2020 (2008).
8 Fthenakis VM, Hyung CK and Alsema E, Emissions from photovoltaic life cycles. *Environ Sci Technol* **42**:2168–2174 (2008).
9 Pacca S, Sivaraman D and Keoleian GA, Parameters affecting the life cycle performance of PV technologies and systems. *Energy Policy* **35**:3316–3326 (2007).
10 Valero D, Ortiz JM, Expósito E, Montiel V and Aldaz A, Electrocoagulation of a synthetic textile effluent powered by photovoltaic energy without batteries: direct connection behaviour. *Sol Energy Mater Sol Cells* **92**:291–297 (2008).
11 Figueroa S, Vázquez L and Alvarez-Gallegos A, Decolorizing textile wastewater with Fenton's reagent electrogenerated with a solar photovoltaic cell. *Water Res* **43**:283–294 (2009).

12 Hyunwoong P, Vecitis CD, Wonyong C, Weres O and Hoffmann MR, Solar-powered production of molecular hydrogen from water. *J Phys Chem C* **112**:885–889 (2008).
13 Thomson M and Infield D, Laboratory demonstration of a photovoltaic-powered seawater reverse-osmosis system without batteries. *Desalination* **183**:105–111 (2005).
14 Cañizares P, Díaz M, Domínguez JA, García-Gómez J and Rodrigo MA, Electrochemical oxidation of aqueous phenol wastes on synthetic diamond thin-film electrodes. *Ind Eng Chem Res* **41**:4187–4194 (2002).
15 Panizza M, Michaud PA, Cerisola G and Comninellis C, Electrochemical treatment of wastewaters containing organic pollutants on boron-doped diamond electrodes: prediction of specific energy consumption and required electrode area. *Electrochem Commun* **3**:336–339 (2001).
16 Bonvin G and Comninellis C, Scale-up of bipolar electrode stack dimensionless numbers for current bypass estimation. *J Appl Electrochem* **24**:469–474 (1994).
17 Yaws CL, *Yaws' Handbook of Thermodynamic and Physical Properties of Chemical Compounds*. Knovel, Norwich, New York (2003).
18 Celik AN and Acikgoz N, Modelling and experimental verification of the operating current of mono-crystalline photovoltaic modules using four- and five-parameter models. *Appl Energy* **84**:1–15 (2007).
19 Townsend TU, Simplified performance modeling of a direct-coupled photovoltaic systems. Master's thesis, University of Wisconsin, Madison (1989).
20 Gow JA and Manning CD, Development of a photovoltaic array model for use in power-electronics simulation studies. *IEE Proc Elec Power Appl* **146**:193–200 (1999).
21 Ortiz JM, Expósito E, Gallud F, García-García V, Montiel V and Aldaz A, Electrodialysis of brackish water powered by photovoltaic energy without batteries: direct connection behaviour. *Desalination* **208**:89–100 (2007).
22 Ortiz JM, Expósito E, Gallud F, García-García V, Montiel V and Aldaz A, Photovoltaic electrodialysis system for brackish water desalination: modeling of global process. *J Membr Sci* **274**:138–149 (2006).
23 Bolton JR, Bircher KG, Tumas W and Tolman CA, Figures-of-merit for the technical development and application of advanced oxidation technologies for both electric- and solar-driven systems. *Pure Appl Chem* **73**:627–637 (2001).
24 California Energy Commission, California's water – energy relationship CEC-700-2005-011-SF (2005).
25 European Commission, Reference document on best available techniques in common waste water and waste gas treatment/management systems in the chemical sector (2007). Available at ftp://ftp.jrc.es/pub/eippcb/doc/cww_bref_0203.pdf (accessed in 2009).
26 Tchobanoglous G, Burton FL and Stensel HD, *Wastewater Engineering: Treatment and Reuse*. 4th edn. McGraw-Hill, Boston, 1819 (2003).
27 Cañizares P, Martínez L, Paz R, Sáez C, Lobato J and Rodrigo MA, Treatment of Fenton-refractory olive oil mill wastes by electrochemical oxidation with boron-doped diamond anodes. *J Chem Technol Biotechnol* **81**:1331–1337 (2006).
28 Cañizares P, Paz R, Lobato J, Sáez C and Rodrigo MA, Electrochemical treatment of the effluent of a fine chemical manufacturing plant. *J Hazard Mater* **138**:173–181 (2006).
29 Malpass GRP, Miwa DW, Mortari DA, Machado SAS and Motheo AJ, Decolorisation of real textile waste using electrochemical techniques: effect of the chloride concentration. *Water Res* **41**:2969–2977 (2007).
30 Dominguez-Ramos A, Aldaco R and Irabien A, Electrochemical oxidation of lignosulfonate: total organic carbon oxidation kinetics. *Ind Eng Chem Res* **47**:9848–9853 (2008).
31 Serrano K, Michaud PA, Comninellis C and Savall A, Electrochemical preparation of peroxodisulfuric acid using boron doped diamond thin film electrodes. *Electrochim Acta* **48**:431–436 (2002).
32 Michaud P, Mahé E, Haenni W, Perret A and Comninellis C, Preparation of peroxodisulfuric acid using boron-doped diamond thin film electrodes. *Electrochem Solid-State Lett* **3**:77–79 (2000).
33 Marselli B, Garcia-Gomez J, Michaud PA, Rodrigo MA and Comninellis C, Electrogeneration of hydroxyl radicals on boron-doped diamond electrodes. *J Electrochem Soc* **150**:D79–83 (2003).
34 Kapalka A, Fóti G and Comninellis C, Kinetic modelling of the electrochemical mineralization of organic pollutants for wastewater treatment. *J Appl Electrochem* **38**:7–16 (2008).
35 DeLucas A, Cañizares P, Rodrigo MA and García-Gómez J, Electrochemical treatment of aqueous phenol wastes: A preliminary economical outlook. *Waste Manag Environ* 161–170 (2002).
36 Cañizares P, Paz R, Sáez C and Rodrigo MA, Costs of the electrochemical oxidation of wastewaters: A comparison with ozonation and Fenton oxidation processes. *J Environ Manage* **90**:410–420 (2009).
37 Fiorenza G, Sharma VK and Braccio G, Techno-economic evaluation of a solar powered water desalination plant. *Energy Conv Manage* **44**:2217–2240 (2003).
38 Palmas S, Polcaro AM, Vacca A, Mascia M and Ferrara F, Influence of the operating conditions on the electrochemical disinfection process of natural waters at BDD electrodes. *J Appl Electrochem* **37**:1357–1365 (2007).
39 Jeong J, Kim JY and Yoon J, The role of reactive oxygen species in the electrochemical inactivation of microorganisms. *Environ Sci Technol* **40**:6117–6122 (2006).
40 Kerwick MI, Reddy SM, Chamberlain AHL and Holt DM, Electrochemical disinfection, an environmentally acceptable method of drinking water disinfection? *Electrochim Acta* **50**:5270–5277 (2005).
41 Diao HF, Li XY, Gu JD, Shi HC and Xie ZM, Electron microscopic investigation of the bactericidal action of electrochemical disinfection in comparison with chlorination, ozonation and fenton reaction. *Process Biochem* **39**:1421–1426 (2004).
42 Pelegrini RT, Freire RS, Duran N and Bertazzoli R, Photoassisted electrochemical degradation of organic pollutants on a DSA type oxide electrode: process test for a phenol synthetic solution and its application for the E1 bleach kraft mill effluent. *Environ Sci Technol* **35**:2849–2853 (2001).
43 EU PV Technology Platform, Working Group 3, *Science, Technology and Applications, A strategic research agenda for photovoltaic solar energy technology* (2007).
44 Panizza M, Kapalka A and Comninellis C, Oxidation of organic pollutants on BDD anodes using modulated current electrolysis. *Electrochim Acta* **53**:2289–2295 (2008).

